Molecular Modeling of Spider Silk Elasticity

Yves Termonia

Central Research and Development, Experimental Station, E. I. du Pont de Nemours Inc., Wilmington, Delaware 19880-0356

Received June 6, 1994; Revised Manuscript Received September 1, 1994[⊗]

ABSTRACT: We introduce the first comprehensive molecular model of spider dragline elasticity which clearly integrates most of the information known to date about the structure of the fiber. In accordance with X-ray evidence, the dragline is represented by a large number of small crystallites separated by amorphous regions made of rubber-like chains. Our model results clearly indicate the important role of the crystallites which act as multifunctional cross-links and create inside the amorphous regions a thin layer with modulus higher than in the bulk. The role of the crystallites in spider silk is found to be amazingly similar to that speculated for carbon black in synthesized elastomers.

1. Introduction

The pressure of natural selection has made spider dragline silk one of the most attractive materials available to date.[1−6] The fiber is stronger than steel and has a tensile strength approaching that of Kevlar. Unlike the latter, however, spider silk is also characterized by an extremely high elasticity. That unusual combination of high strength and stretch leads to toughness values never attained in synthetic high-performance fibers. Other attractive features of spider silk include excellent compressive properties, ease of dyeability, extensive softening and supercontraction in humid environments, and foremost the ability to easily dissolve in aqueous solutions at room temperature. The latter is in contrast to synthetic fibers which, for comparable performance, require processing in very caustic solvents and/or at elevated temperatures. High-strength synthetic fibers also require a postspinning draw of several hundred percent, which is totally absent in spider silk dragline.

Within the past few years, there has been a renewed interest in the use of natural fibers for commercial applications, particularly in view of the urgent need for environmentally sound materials.[7] Spurred on by new advances in protein biosynthesis and a recent identification of the amino acid sequence of spider silk DNA,[8,9] several researchers have turned to the synthesis of silk analogs, using fermentation in genetically altered bacteria.[10,11] The harnessing of bacteria for commercial polymer synthesis however still remains plagued by a poor control of the molecular weight distribution and an extremely low product yield due to proteolysis.

From a theoretical standpoint, little progress has been made regarding our understanding of the structure−property relationships in spider silk. The silk has been, for more than 30 years,[12] clearly identified as a semicrystalline polymer resembling most synthetic man-made fibers but the origin of its exceptional mechanical properties still remains obscure. It is the purpose of the present work to provide some insight into the molecular mechanism of spider silk elasticity and strength. Such an understanding is of fundamental importance for guiding experimental research toward the synthesis and design of synthetic materials which would either mimic or improve on spider silk properties.[13]

[⊗] Abstract published in *Advance ACS Abstracts,* October 15, 1994.

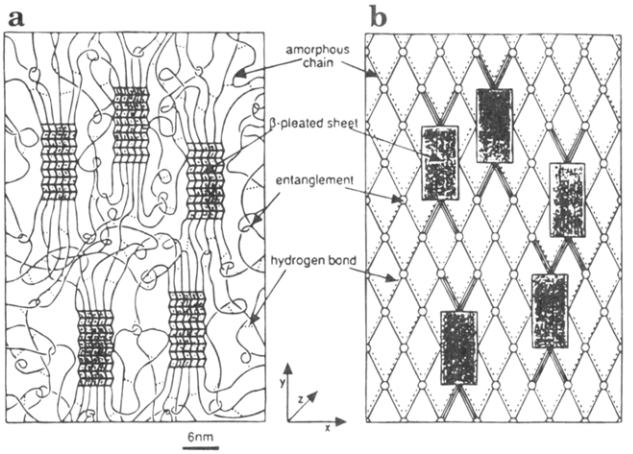

Figure 1. Left: Model of the dry dragline. For the purpose of easy representation, the figure is for a 15% volume fraction of β-pleated sheets. Right: More schematic representation in which the details of the amorphous chains have been omitted and only end-to-end vectors are shown. Individual hydrogen bonds have been replaced by "overall" bonds (dotted lines) connecting every entanglement to its neighbors. The three-line vectors indicate the high-modulus layer in the amorphous phase.

2. Model

As stated in the Introduction, it is now well accepted that spider dragline is a semicrystalline material made of amorphous flexible chains reinforced by strong and stiff crystals. These crystals are believed to be made of hydrophobic polyalanine sequences arranged into hydrogen-bonded β-pleated sheets which run parallel to the fiber axis.[14,15] The amorphous part, on the other hand, can be attributed to kinetically free oligopeptide chains rich in glycine. (For simplicity, we do not consider the possibility of helix formation in the amorphous phase.[16]) For a typical 40% volume fraction of β-sheets, the free oligopeptide chains contain on the average 63 bond angles along the backbone, and their length is therefore comparable to the entanglement spacing in synthetic polyethylene.[17] In addition to being entangled, the amorphous chains are also linked together through hydrogen bonds which give the fiber its high initial modulus.[18] The above considerations lead to the schematic representation in Figure 1a of a dragline containing about 15% β-pleated sheets by volume. Since the coordination number of an entanglement is only 4, our model is restricted to a two-dimensional geometry including no more than one β-sheet of each crystallite. For simplicity, we also omit

0024-9297/94/2227-7378$04.50/0

the details of the configurations of the amorphous chains between entanglements and our model structure is further simplified as in Figure 1b. In that new representation, the entanglements are arranged on a regular lattice of nodes connected by the end-to-end vectors of the chain strands. That simplification also leads to the replacement of the hydrogen bonds along chains by "overall" bonds (dotted lines) further connecting each entanglement to its neighbors. Note that a similar model representation has been used in a previous analysis of the factors controlling the deformation behavior of semicrystalline polyethylene.[19]

A last and important remark has to be devoted to the role of the crystalline β-sheets. X-ray diffraction studies[1,14] have determined that the crystallites are elongated along the fiber axis and have lateral dimensions of 2 nm along the z-direction and 6 nm along the transverse x-axis; see Figure 1a. Although these dimensions are for *Bombyx mori* coccoon silk, data for the spider dragline should not be too different. Further study reveals that up to 60 chains can be accommodated in a crystallite with these lateral dimensions.[14] The β-sheets therefore can be viewed as multifunctional cross-links which create inside the amorphous region a thin layer with a modulus of elasticity higher than in the bulk. The effective thickness of that layer is of the order of the end-to-end vector length of the trapped chains.[20] Since chains trapped within a confined geometry do not lose their extensibility,[21] that length is about the same as that between entanglements in the bulk, i.e. approximately 5 nm for most rubber-like polymers.[20] The presence of a rubbery layer of higher modulus has been schematically represented in Figure 1b through the use of a three-line vector length for the chain strands. As will be discussed later, the reinforcing effect of the β-sheets in spider silk is very similar to that attributed to carbon black in synthesized elastomers.[22]

More information about the structure of spider silk can be learned from the effect of water on its components. Water is well known to have a plasticizing effect on the amorphous phase by preventing the formation of hydrogen bonds between chains. No effect, however, has been reported on the hydrophobic crystalline β-sheets.[23,24] The plasticizing role of water is of great importance in the fiber spinning process which is performed from an aqueous solution. In the postspinning stage, the fiber is dried in the stressed state which then allows hydrogen bonds to re-form between amorphous chains and lock-in their orientation and stretch. That residual stress is responsible for the 50% shrinkage of the dragline when reexposed to water.[2,23] The potential for supercontraction in the dry dragline can be easily implemented in our model of Figure 1. We start with the "wet" structure in which hydrogen bonds are absent and the amorphous chains assume a random coil configuration. That structure is stretched on the computer to a draw ratio $\lambda \approx 2$ and the orientation induced in the amorphous chains is then frozen-in through the imposition of hydrogen bonds between nodes (dotted lines in Figure 1b).

2.1. Model Parameters. The model parameters can be determined as follows. The elastic tensile modulus of the hydrogen bonds is set equal to $E_h = 4$ GPa, a value typical for hydrogen-bonded chains.[29] For the crystalline β-sheets, we take $E_c = 160$ GPa.[25] As alluded to earlier, the elastic properties of the amorphous chains can be approximated by those of synthetic polyethylene.[19] Thus, the molecular weight between entanglements M_e is in the range 1500–2000, which corresponds to $n_e \approx 14$ statistical segments, each of length $l = 1$ nm.[19] In a wet unrestrained fiber, the end-to-end vector length between entanglements therefore equals

$$r_0 = l n_e^{1/2} = 3.7 \text{ nm} \tag{1}$$

For simplicity, we shall not in the present paper consider the possibility of chain slippage through entanglements, although the process could be easily implemented.[19] An estimate of the elastic modulus E_a of the amorphous chain strands between entanglements can be obtained as follows. Taking a density $\varrho = 1.347$ (ref 26) together with $M_e = 1500$ leads to $N = 5.4 \times 10^{26}$ strands/m^3. The elastic tensile modulus can then be calculated from

$$E_a = 3NkT \approx 7 \text{ MPa} \tag{2}$$

in which the right-hand side is the value obtained at room temperature. The modulus value in the amorphous layer close to the β-sheets (three-line strands in Figure 1b) is somewhat more difficult to determine. Since a β-pleated sheet contains 12 chains,[14] each of the two (three line) strands emanating from a β-sheet has been given a modulus value $E_{layer} = 6E_a$. That high value reflects the constrainment of the chains exiting each sheet and, as will be clearly demonstrated in section 3, it is also responsible for the unusual mechanical properties of the dragline.

2.2. Tensile Deformation and Fracture. Having determined the parameter values for the dragline, its mechanical properties are obtained as follows. (For more general details on our technique, the reader is referred to ref 19.) The network of Figure 1b is deformed at a constant rate of elongation $\dot{\epsilon}$ in a series of small strain increments $\delta\epsilon$. For every small strain increment, the elastic network is relaxed to its minimum energy configuration using a series of fast computer algorithms which steadily decrease the net residual stress acting on each lattice node.[27] In that process, the stress on a hydrogen or a crystalline bond i is obtained from

$$\sigma_i = E_i \epsilon_i \tag{3}$$

in which E_i (=E_h or E_c) and ϵ_i are the local modulus and strain, respectively. For an amorphous chain strand i, we use[28]

$$\sigma_i = E_a n_e^{1/2} (1/3) \mathcal{L}^{-1}[\lambda_i / n_e^{1/2}] - \sigma_0 \tag{4}$$

where $\mathcal{L}^{-1}$ is the inverse Langevin function and $\lambda_i = (1 + \epsilon_i)$ denotes the local draw ratio. σ_0 in eq 4 represents the stress in the absence of strain, i.e., that for which $\lambda = 1$. Since the lattice is made of stiff crystalline and soft amorphous bonds, the relaxation process described above leads to a very nonaffine deformation of the network. To save computer time, only displacements of the lattice nodes along the tensile y-axis are explicitly calculated. Distances in the transverse x-direction are assumed to be contracted homogeneously by a factor λ^{-1}, where λ is the overall draw ratio along the y-axis.[19]

As the strain on the network increases, the amorphous chains break when their local draw ratio exceeds its maximum value $\lambda_{max} = n_e^{1/2}$. Hydrogen bonds deform and break at a rate[27–29]

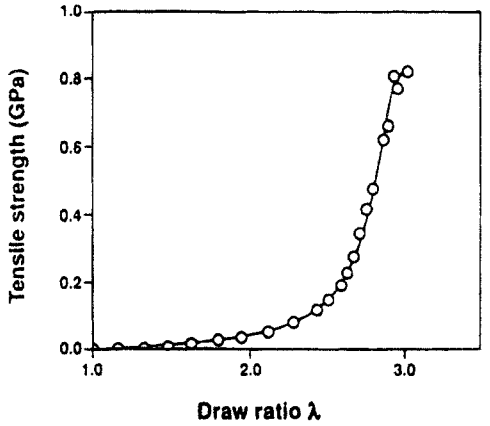

Figure 2. Calculated stress *vs* draw ratio curve for the unrestrained wet dragline (○). The figure is for a volume fraction of crystallites $v_c = 0.45$ and a rate of strain $\dot{\lambda} = 1.42$/min. The curve is drawn to guide the eye.

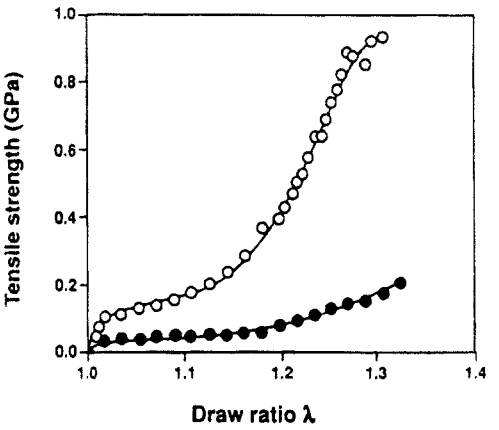

Figure 3. Calculated stress *vs* draw ratio curve for the dry dragline (○). Model parameters are the same as for Figure 2. The structure of the dry dragline was obtained after stretching a "wet" dragline to $\lambda_s = 2.3$ and allowing hydrogen bonds to form within the amorphous phase. Also represented (●) are our model predictions for the case $E_{layer} = E_a$; see text.

$$v_i = \tau \exp[-(U - \beta\sigma_i)/kT] \qquad (5)$$

where σ_i is the local stress, τ is the thermal vibration frequency, and U and β are the activation energy and volume, respectively. In our process, we use $U = 35$ kcal/mol,[29] which ensures that the cooperative breaking of these "overall" bonds readily occurs, in the absence of stress, at temperatures above 250 °C, which is in the range of melting temperatures for spider dragline[30] and other hydrogen-bonded flexible polymers such as nylon-6. We also choose $\beta = (4.74\ \text{Å})^3$, which ensures hydrogen bond breakage near the experimental "yield" point found at about 2% strain.[26] As an "overall" hydrogen bond breaks, the load it carries is transferred to the underlying amorphous chain strand whose local stress is then calculated from eqs 2 and 4.

For simplicity, we assume no breaking of the crystallites. That assumption is supported by our observation (see later) that, because of their high stiffness, the β-sheets are never strained by more than 2–3%, a value too low for covalent bond breaking.[29] All the results to be presented below are for a volume fraction of crystallites $v_c = 0.45$, which is in the range of values found experimentally.[31,32]

3. Results and Discussion

3.1. Wet Unrestrained Dragline. We start by presenting our model results for the wet dragline whose behavior should also be similar to that of the coated capture thread.[5] In our model of the wet unrestrained dragline, we assume that the only effect of water on the structure of Figure 1 is to prevent the formation of hydrogen bonds within the proteins and to give the amorphous chains an isotropic random coil configuration. Swelling effects are neglected. Figure 2 shows our model prediction (symbol ○) for the dependence of stress on draw ratio λ for the unrestrained wet dragline. The strain rate is set at $\dot{\lambda} = 1.42$/min. Inspection of the figure shows that the stress–strain curve is linear up to $\lambda \approx 2$, with a modulus value of about 30 MPa. That value is about 3 times lower than that reported for viscid silk,[33] probably because of transient interchain bonds present in the experimental fiber.[34] At higher $\lambda > 2$, our calculated modulus value increases sharply with strain, in perfect agreement with experimental observation.[26,33] At still higher $\lambda > 2.8$, our model results indicate that the rubber-like chains in the amorphous region progressively reach full extension and break, as indicated by the turning down of the stress–strain curve. That process eventually leads, near $\lambda = 3$, to catastrophic failure of the fiber. Further investigation also reveals that the strain in the β-sheets never exceeds 2–3%, which justifies our neglect of covalent bond breaking in the crystalline phase.

3.2. Dry Dragline. Figure 3 shows our calculated stress–strain curve (symbol ○) for the dragline in the dry state. As for Figure 2, the curve is for a volume fraction of crystallites $v_c = 0.45$ and a rate of strain $\dot{\lambda} = 1.42$/min. At small strains ($\lambda < 1.02$), the stress–strain curve is linear with modulus $E = 10$ GPa, in perfect agreement with experimental observation.[3] At $\lambda \cong 1.02$, our model results indicate the onset of breaking of the hydrogen bonds between chains in the amorphous regions. That process leads to the formation of a so-called "yield point"[19] at which the stress–strain curve reaches a plateau. At higher $\lambda > 1.1$, the hydrogen bond breaking process is almost complete and the stress resumes its increase with strain. At that stage, the structure of a dry dragline is very similar to that of its wet counterpart and the two stress–strain curves almost superimpose (compare Figures 2 and 3). Note that our model results predict a 30% elongation at break together with a tensile strength approaching 1 GPa, in excellent agreement with experimental observation.[26,33]

3.3. Role of the Crystallites and Their Size. The results of Figures 2 and 3 fully take into account the reinforcing effect of the β-crystallites which create inside the amorphous region a thin layer with modulus higher than in the bulk, i.e., $E_{layer} = 6E_a$. Thus, also represented in Figure 3 are our model predictions for the case $E_{layer} = E_a$ (symbol ●). The results reveal a substantial decrease in modulus and in tensile strength, which in turn indicates the crucial role played by that high-modulus layer. An important remark on the reinforcement efficiency of the latter is in order. As has been discussed earlier, the thickness of the high-modulus layer around the crystallites is equal to the average distance between entanglements, which, for most flexible polymers, is of the order of 5 nm.[20] In order for that thin layer to be effective, its volume fraction in the dragline must be high, which in turn requires that the crystallites be not too large. The effect of the crystallite size is studied in Figure 4 for a constant volume fraction $v_c = 0.45$. Our data for the dry dragline with its small $2 \times 6 \times 21$ nm crystallites are reproduced from Figure 3 (symbol ○). Model predictions with crystallites 9

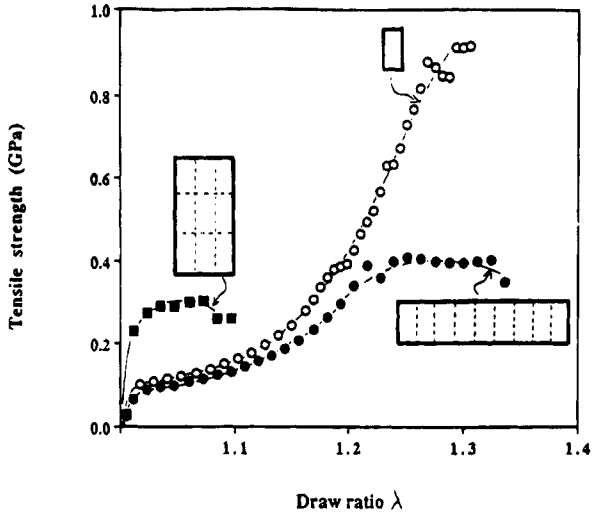

Figure 4. Effect of crystallite size on stress–strain curve. Our data for the dry dragline with its small 2 × 6 × 21 nm crystallites are reproduced from Figure 3 (○). Model predictions with crystallites 9 times larger are denoted by (●) and (■) for two different aspect ratios; see figure. Other model parameters are the same as in Figure 3.

times larger are denoted by symbols ● and ■ for two different aspect ratios; see figure. Our data clearly indicate that an increase in crystallite size leads to a substantial decrease in tensile strength. At small aspect ratios (symbol ●), that decrease is due to a lowering of the modulus whereas at high aspect ratios (symbol ■) it is attributed to a dramatic drop in elongation at break.

From our model results of Figures 3 and 4, it appears that the β-crystallites in the dragline have an optimum size. Thus, on one hand, the crystals are small enough to ensure a high volume fraction of the thin reinforcing layer whereas, on the other, they are also large enough to guarantee a high modulus for that layer ($E_{layer} = 6E_a$). As stated earlier, there exists a surprising similarity between the reinforcing effect of the β-crystallites in spider dragline and that of carbon black in synthesized rubbers.[22] Carbon black particles indeed have diameters no larger than 20–30 nm and, as for the dragline, they typically lead to the formation inside the rubber of a thin interphase, 3 nm thick, in which the mobility of the chains is very constrained.[22] The importance of these interphases has been widely anticipated in synthetic semicrystalline polymers.[35–37] To the best of our knowledge, the present approach is, however, the first one to clearly demonstrate and quantify the dramatic improvement in mechanical properties brought upon by the addition of very small crystals to a rubbery matrix.

4. Conclusions

In summary, we have presented a molecular model of spider silk elasticity which clearly integrates most of the information known to date about the structure and the elastic behavior of the fiber. Since data on the amorphous phase of the fiber are rather sketchy, that phase has been for simplicity attributed the properties of coiled polyethylene chains which have been well characterized from previous work.[19] Our model has been quite successful in reproducing the complex stress–strain curves found experimentally for the dragline in both the wet and the dry states. The supercontraction phenomenon has also been fully accounted for. More importantly, our approach provides the first comprehensive analysis of the factors controlling spider silk elasticity. In that connection, our model clearly reveals the importance of the crystalline β-sheets which create inside the amorphous phase a thin layer with modulus higher than in the bulk.

We are perfectly aware that the present model may be too simplistic to describe all the aspects of spider silk elasticity. The approach, however, brings out very clearly essential points like the effect of water and the role of the crystalline and amorphous phases. It is our hope that such a simplified approach will foster further theoretical and experimental research aimed at designing synthetic materials which would either mimic or improve on spider silk properties.

Acknowledgment. I wish to thank Drs. John P. O'Brien and Kenn C. Gardner for introducing me into the field of spider silk structure and elasticity.

References and Notes

(1) Denny, M. W. In *The Mechanical Properties of Biological Materials, Symposia of Society for Experimental Biology*; Cambridge University Press: Cambridge, 1980; Vol. 34, pp 247–272.
(2) Gosline, J. M.; Denny, M. W.; DeMont, M. E. *Nature* **1984**, *309*, 551.
(3) Gosline, J. M.; DeMont, M. E.; Denny, M. W. *Endeavor* **1986**, *10*, 37.
(4) Calvert, P. *Nature* **1989**, *340*, 266.
(5) Vollrath, F.; Edmonds, D. T. *Nature* **1989**, *340*, 305.
(6) Kerkam, K.; Viney, C.; Kaplan, D.; Lombardi, S. *Nature* **1991**, *349*, 596.
(7) Timmins, M. R.; Lenz, R. W. *Trends Polym. Sci.* **1994**, *2*, 15.
(8) Xu, M.; Lewis, R. V. *Proc. Natl. Acad. Sci. U.S.A.* **1990**, *87*, 7120.
(9) Lewis, R. V. *Acc. Chem. Res.* **1992**, *25*, 392.
(10) Capello, J.; McGrath, K. P. *ACS Symp. Ser.* **1994**, *544*, 311.
(11) O'Brien, J. P. *TRIP* **1993**, *1*, 228.
(12) Warwicker, J. O. *J. Mol. Biol.* **1960**, *2*, 350.
(13) Ball, P. *Nature* **1994**, *367*, 323.
(14) Fraser, R. D. B.; MacRae, T. P. *Conformation in Fibrous Proteins*; Academic Press: New York, 1973; p 317.
(15) Gardner, K. H., private communication.
(16) Hinman, M. B.; Lewis, R. V. *J. Biol. Chem.* **1992**, *267*, 19320.
(17) Ferry, J. D. *Viscoelastic Properties of Polymers*, 3rd ed.; John Wiley & Sons: New York, 1980; p 374.
(18) Lucas, F.; Shaw, J. T. B.; Smith, S. G. *Shirley Inst. Mem.* **1955**, *28*, 77.
(19) Termonia, Y.; Smith, P. *Macromolecules* **1987**, *20*, 835; **1988**, *21*, 2184; **1988**, *21*, 3485; **1993**, *26*, 3738.
(20) Flory, P. J. *Principles of Polymer Chemistry*; Cornell University Press: Ithaca, NY, 1983; p 481.
(21) de Gennes, P.-G. *Scaling Concepts in Polymer Physics*; Cornell University Press: Ithaca, NY, 1985; p 34.
(22) Donnet, J. B.; Vidal, A. In *Pharmacy, Thermomechanics, Elastomers, Telechelics*; Dusek, K., Ed.; Springer-Verlag: Berlin, 1986; pp 104–127.
(23) Fornes, R. E.; Work, R. W.; Morosoff, N. *J. Polym. Sci., Polym. Phys. Ed.* **1983**, *21*, 1163.
(24) Bonthrone, K. M.; Vollrath, F.; Hunter, B. K.; Sanders, J. K. M. *Proc. R. Soc. London, B* **1992**, *248*, 141.
(25) Iizuka, E. *Biorheology* **1965**, *3*, 1.
(26) Work, R. W. *Textile Res. J.* **1977**, *47*, 650.
(27) Termonia, Y.; Meakin, P.; Smith, P. *Macromolecules* **1985**, *18*, 2246.
(28) Termonia, Y. *Macromolecules* **1989**, *22*, 3633.
(29) Termonia, Y.; Smith, P. *Polymer* **1986**, *27*, 1845.
(30) Cunniff, P. M.; Fossey, S. A.; Auerbach, M. A.; Song, J. W. *ACS Symp. Ser.* **1994**, *544*, 234.
(31) Iuzuka, E. *J. Appl. Polym. Sci.: Appl. Polym. Symp.* **1985**, *41*, 173.
(32) Gillespie, D. B.; Viney, C.; Yager, P. *ACS Symp. Ser.* **1994**, *544*, 155.
(33) Denny, M. *J. Exp. Biol.* **1976**, *65*, 483.
(34) That interpretation is supported by the fact that, after a few loading cycles, the experimental modulus decreases and becomes closer to our calculated value.
(35) Flory, P. J.; Yoon, D. Y. *Nature* **1978**, *272*, 226.
(36) Flory, P. J.; Yoon, D. Y.; Dill, K. A. *Macromolecules* **1984**, *17*, 862.
(37) Marqusee, J. A. *Macromolecules* **1989**, *22*, 472.